AGU ADVANCING EARTH AND SPACE SCIENCE

Earth and Space Science

RESEARCH ARTICLE
10.1029/2021EA002167

Evolution of Fractal Pore Structure in Sedimentary Rocks

Nengwu Zhou[1], Min Wang[1], Shuangfang Lu[1], Thomas J. H. Dodd[2], Wei Liu[1], and Ying Guan[1]

[1]Key Laboratory of Deep Oil and Gas, China University of Petroleum (East China), Qingdao, China, [2]British Geological Survey, The Lyell Centre, Edinburgh, UK

Key Points:

- Evolution of fractal dimension with diagenesis was revealed
- Effects of diagenesis on fractal upper and lower limits were discussed
- Effect mechanism of fractal pore structure was revealed in sedimentary rocks

Correspondence to:

M. Wang and S. Lu,
wangm@upc.edu.cn;
lushuangfang@upc.edu.cn

Citation:

Zhou, N., Wang, M., Lu, S., Dodd, T. J. H., Liu, W., & Guan, Y. (2022). Evolution of fractal pore structure in sedimentary rocks. *Earth and Space Science*, *9*, e2021EA002167. https://doi.org/10.1029/2021EA002167

Received 12 DEC 2021
Accepted 20 MAY 2022

Author Contributions:

Conceptualization: Nengwu Zhou, Min Wang, Shuangfang Lu
Data curation: Wei Liu, Ying Guan
Formal analysis: Nengwu Zhou
Funding acquisition: Min Wang, Shuangfang Lu
Investigation: Nengwu Zhou
Methodology: Nengwu Zhou, Wei Liu, Ying Guan
Resources: Min Wang, Shuangfang Lu
Supervision: Min Wang, Shuangfang Lu
Writing – original draft: Nengwu Zhou
Writing – review & editing: Nengwu Zhou, Thomas J. H. Dodd

Abstract Geological processes alter pore spaces over time, and their analysis can shed light on the dynamic fractal structure and fluid flow of rocks over time. This study presents experimental evidence to illustrate that the pore fractal structure evolves with sedimentation, carbonate cementation, clay growth, and dissolution. It examines, describes and characterizes a suite of core samples from the Gaotaizi oil layer of the second and third members of the Qingshankou Formation, Songliao Basin, China. The effects of mechanical compaction and other diagenesis effects on fractal pore structure on sedimentary rocks are discussed. A schematic diagram is proposed that describes the impacts of these diagenetic processes on fractal pore structure at the microscopic scale in sedimentary rocks. This work links the state of diagenetic alteration and fractal pore structure, which can guide practical applications such as predicting the permeability of sedimentary rocks.

Plain Language Summary Mechanical compaction or chemical alteration process will change the pore space of the rock, including pore size and grain-pore interface properties. We present the evidence that geological processes alter the "roughness" amplitude of grain-pore interface (fractal pore structure) in sedimentary rock, and discuss the evolutionary mechanism of the "roughness" amplitude of grain-pore interface. This work links the state of diagenetic alteration and fractal properties of rocks, which can guide practical applications such as predicting permeability of sedimentary rocks for any historical period.

1. Introduction

The "fractal" has proven to be a highly useful method to describe the statistics of the geometric shapes of natural objects occurring in time and space, and is often used when considering geoscience topics such as the boundaries of mountains and coastlines (Thompson, 1991) and is often applied to fluid-flow analysis (Yu et al., 2014). Commonly, sedimentary rocks form the porous medium in which fluid (i.e., oil and gas) is often contained. Understanding fluid flow into, and within sandstone reservoirs, and the ability to better appraise their storage capacity are significant for the migration and accumulation of oil and gas reserves (Lu et al., 2016, 2018). However, the complexity and irregularity of microscopic structures at the pore-scale often make grain-pore interface morphology difficult to quantitatively characterize using traditional Euclidean geometry (Daigle et al., 2014; Wang et al., 2012). Analysis of fractal properties of porous sedimentary rocks at the microscopic scale can help characterize, and ultimately successfully predict single phase fluid flow (Cai et al., 2019; Chen & Yao, 2017; Costa, 2006; Vadapalli et al., 2014; Wei et al., 2015), two-phase fluid flow (Cihan et al., 2009; Li & Horne, 2006; Liu, 2007; Wang, Guan, et al., 2020; Zhang et al., 2020, 2021), and even multiphase fluid flow (Moulu et al., 1997; Yang & Mohanty, 2015). However, as pore space becomes altered over geological time, these experimental data do not reflect the transport properties of historical periods.

The fluid flow within sedimentary rocks depends on the pore size and grain-pore interface morphology, which are altered over geological time by fluid-rock interactions. Grain-pore interface properties, such as roughness, also evolve dynamically and consequently become indicators of the sedimentary rock formation history (Aharonov & Rothman, 1996). The pore space character is controlled by primary sedimentation and subsequent process such as compaction and diageneses. Primary sedimentary processes determine the initial pore space configuration, which is then altered by the diagenetic process through mechanical compaction and fluid-rock interaction (Anovitz et al., 2013; Emmanuel et al., 2015; Qiao et al., 2020; Wang et al., 2017). Resulting pore structures determine the fluid flow potential of the forming rock. Previous studies have focused on the alteration of pore size (Emmanuel et al., 2010, 2015; Stack, 2015), rather than pore surface morphology, of which more understanding and characterization is required.

Experimental measurements, using a variety of techniques (i.e., fracture surface technique, scanning electron microscopy, small-angle neutron scattering, mercury intrusion capillary pressure, gas adsorption, nuclear magnetic resonance, micro-CT), have shown that the grain-pore interfaces exhibit a fractal structure in most sedimentary rocks, from the nanoscale to the grain scale (Anovitz et al., 2015; Avnir et al., 1984; Daigle et al., 2014; Katz & Thompson, 1985; Rahner et al., 2018; Thompson et al., 1987; Wang et al., 2015; Zhou et al., 2020). Fractal pore structure includes the "fractal dimension" describing the geometrical properties of a pore space, such as its roughness (Issa et al., 2003; Nigon et al., 2017; Power & Tullis, 1991) and the "fractal boundary" (upper and lower limit) referring to the pore size range exhibited fractal behavior (Krohn, 1988). Thompson et al. (1987) pointed out that the crystal growth and dissolution processes may produce fractal growth on pore surfaces, and that the "fractal dimension" of pore surfaces can be correlatable to the level of chemical diagenesis.

Therefore, clarifying the evolution of fractal pore structure will not only deepen the knowledge of the alternation on micropore geometry (especially the nature of the interface properties), but also provides a possible guide to predict the fluid flow of sedimentary rocks. This study provides important insights into pore structures and pore-grain interfaces though microscope observation techniques (thin section and scanning electron microscopy) and pore structure characterization techniques (low-field nuclear magnetic resonance). Through this analysis, this study answers the following key questions:

1. How does the fractal pore structure evolve with diagenesis?
2. What is the mechanism of the evolution of fractal pore structure with diagenesis?

By answering these questions, this study provides comment on the effects of mechanical compaction, and chemical diagenetic processes on the fractal properties of host sedimentary rocks. This works links the state of diagenetic alteration with the fractal properties of rocks, and ultimately provides an important insight into potential workflows for the future characterization of fractal structure in potential and known clastic hydrocarbon reservoirs, worldwide.

2. Geological Background

The Songliao Basin, located in northeastern China, is a large-scale (c. 260,000 km^2) diamond-shaped nonmarine sedimentary basin (Figure 1a). It is divided into six key tectonic units, including the central depression, the "northern pitching area," western slope area, and the northeast, southeast, and southwest uplift zones. The study area is located in the northern portion of the central depression, including the Qijiabei, Qijianan, and Longhupao areas, spanning the Qijia-Gulong depression and Longhupao-Da'an terrace, two secondary tectonic units, with a total area of approximately 2,500 km^2 (Figures 1a and 1b). In Cretaceous age, the Songliao Basin was a large lake basin, and oil-producing strata was deposited in this age. In the Lower Cretaceous Quantou Formation and the Upper Cretaceous Qingshankou Formation, six oil layers are distributed from bottom to top, namely Yangda-Chengzi, Fuyu, Gaotaizi, Putaohua, Saertu, and Heidimiao (Figure 1c).

The interval of investigation for this study is within the Gaotaizi oil layer, which belongs to the second and third members of the Qingshankou Formation. During the deposition of the Qingshankou Formation, a regionally extensive transgression event occurred within the Lake that occupied the Songliao Basin during this time (Feng et al., 2009). The first member of Qingshankou Formation represents the deposits of the major transgression, which formed a thick interval (50–250 m) of black gray lacustrine shales. These shales have average values of: 2.5% total organic carbon (TOC) (ranging between 0.11% and 6.95%); average hydrocarbon generation potential ($S_1 + S_2$) of 2.45 mg/g (ranging between 0.04 and 65.33 mg/g); average chloroform bitumen "A" of 0.49% (ranging between 0.01% and 1.75%); and maturity R_o of 0.84% (ranging between 0.37% and 1.42%) (Chen et al., 2014). Following the major transgression, the lake base level continued to advance and retreat, resulting in the interdigitation of delta front and shallow-lacustrine facies, preserved in the rocks of the second and third members of Qingshankou Formation, in the Qijia-Longhupao area (Figure 1c). Sandstones are quite typical within delta front and shallow-lacustrine settings, often interbedded with gray-black and dark gray mudstone layers; the sandstones are thought to be sourced from northerly located areas (Bi et al., 2017; Shi et al., 2015; Wei et al., 2016). The mudstones deposited within members two and three form potential source-rock lithologies, estimated to be between 100 and 450 m in thickness, with source-rock properties of average TOC values of 1.27% (ranging between 0.08% and 6.56%), hydrocarbon generation potential ($S_1 + S_2$) of 28.08 mg/g (0.01–55.40 mg/g),

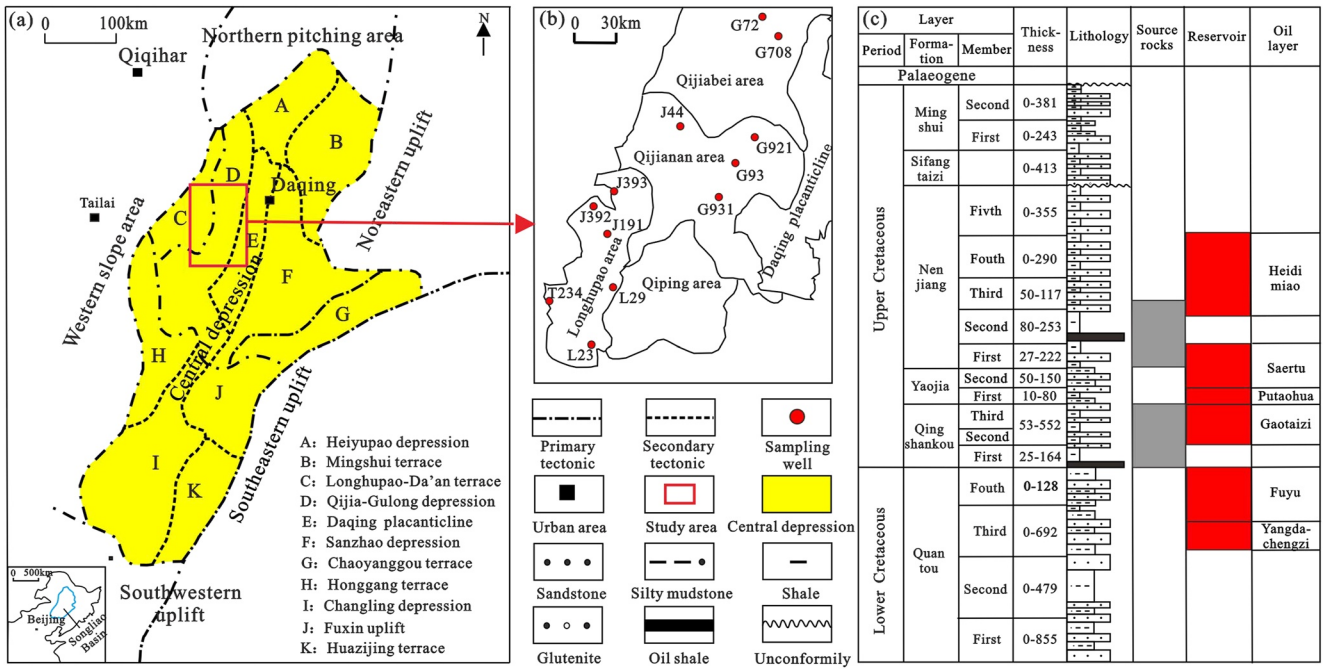

Figure 1. Location information and stratigraphy of the study area. (a) Generalized structural map of the Songliao Basin showing the study area. (b) Detailed information on the study area showing well locations. (c) Stratigraphic column. Figure adapted from Wang, Guan, et al. (2020).

chloroform bitumen "A" of 0.57% (0.01–1.40%), and maturity R_o of 0.81% (ranging between 0.41% and 1.39%) (Chen et al., 2014).

Potential reservoir lithologies form within the delta front areas, typically as sand-prone intervals deposited in shallow-lacustrine environments, within a number of subenvironments that include distributary channels, estuary bars, sheet sands (i.e., strand plains), distal bars, and tributary bays. Internally, each of these subenvironments contains and comprise multiscalar sedimentary layers (beds) of typically 1–2 m in thickness. These sand intervals tend to be laterally extensive, with good continuity, and are sandwiched within mudstone interbeds vertically (Shi et al., 2015).

3. Methodology

3.1. Sample and Experiment

Thirteen full sandstone cores (numbered S1–S13) were sampled from the second and third member of Qingshankou Formation in the Songliao Basin, China (Figure 1b). All cores were washed for 1 week with a mixture of acetone and dichloromethane (3:7) at 90°C with an oil washer. The cores were then dried for 24 hr at 110°C to remove any remaining oil, acetone and dichloromethane. The cores were cut into two parts: regular cylinders (a diameter of 2.5–3 cm and a length of 3–4 cm) and remaining core pieces.

Each cylinder sample was used to conduct routine rock measurements for porosity and permeability, as well as low-field nuclear magnetic resonance (LF-NMR) experiments. The routine rock measurements for porosity and permeability were carried out with a "PorePDP-200" instrument produced by "American CoreLabs." The test pressure during the porosity measurement was 200 Psi, and the test pressure during the permeability measurement was 1,000 Psi. The LF-NMR experiment was carried out at the China University of Petroleum using a "MesoMR23-060H-I" low-field NMR instrument. Samples were tested twice, with the first being to obtain NMR signal of the sample following oil removal and drying, which represents the original signal of the dry sample. The second test simulated formation water (c. 7,000 ppm of salinity), which represents the NMR signal of the dry sample plus pore water. Before the second test, the dry sample is saturated with formation water in a vacuum for at least 24 hr. Based on the first NMR test results, the second NMR test results are inverted to obtain the NMR signal of the fluid in the pore spaces. The testing parameters of the NMR instrument were presented in Table 1.

Table 1
The Testing Parameters of the LF-NMR Experiment

Parameters	Value
Frequency	21.3 MHz
Waiting time	3,000 ms
Echo interval	0.25 ms
Echoes number	12,000
Stacking layers number	64

One part of the remaining cores underwent X-ray diffraction analysis (XRD), which was performed with a "Bruker D8-discover" X-ray diffractometer at the China University of Petroleum that follows Chinese oil and gas industry standards (SY/T 5163-2010). Other parts of the remaining cores underwent two different experiments: thin section analysis (visual inspection and description) and scanning electron microscopy (SEM) analysis for polished and unpolished surface (microscope inspection and description). All microscopic experiments were performed on freshly cut sections. Samples for thin section were mechanically polished, while SEM analysis for polished surface require mechanical and argon ion polishing, and SEM analysis for unpolished surface did not require mechanical or argon ion polishing. Thin section analysis was mainly used to observe the diagenetic mineral present within the rocks. SEM analysis for unpolished surface was used to observe the fresh grain-pore interface of unpolished rock. SEM analysis for polished surface was applied to observe pore structure and its binary image was used to calculate "fractal dimension."

3.2. Fractal Dimension Calculation

In this paper, the "fractal dimension" of the grain-pore interface was measured by the binary image of scanning electron microscopy or thin section using the box-counting method due to its easy implementation and applicability to both self-similar and nonself-similar objects (Ai et al., 2014; Roy et al., 2007). The "fractal dimension" can be derived from the equation below

$$\log(N(\delta)) = D_b \times \log(\delta) + \alpha \tag{1}$$

where $N(\delta)$ is the number of contour boxes, δ the box sizes, and α a proportionality constant. To obtain a more accurate "fractal dimension" D_b value, multiple pictures and different scanning methods are used to avoid the randomness of the "fractal dimension" measured by binarized pictures. Each sample selects four pictures for binarization, and each binarized picture is used to randomly scan 12 times from different areas and directions, the "fractal dimension" of each scan is recorded. This process is automatically finished by the "FracLac" module of the "Image J" software and detailed descriptions and schematic diagram are presented in Figure 2 (Zhou et al., 2020). The "fractal dimension" can be expressed:

$$D_b = \frac{\sum_{i=1}^{i=4} \sum_{j=1}^{j=12} D_{i,j}}{4 * 12} \tag{2}$$

where i is the ith picture, j is the jth scanning, D_{ij} is the "fractal dimension" of the ith picture at the scanning of jth, D_b is the "fractal dimension" of the sample. The calculation results of the "fractal dimension" are shown in Table 2.

3.3. Diagenetic Levels Model

Mineral compaction, precipitation, and dissolution are the three prominent processes to alter the pore space in sedimentary rocks (Emmanuel et al., 2015). The impact of mineral compaction on the reservoir pore space can be characterized by the compaction curve or the depth of burial (Athy, 1930; Guo et al., 2013). Although crystal growth and dissolution rate can be an indicator to evaluate the level of precipitation and dissolution on minerals (Emmanuel et al., 2015; Thompson, 1991; Thompson et al., 1987), they cannot be used to assess diagenetic effects in the rock due to the various reaction rates of the minerals and accessible mineral surface areas of the grain-pore interface (Beckingham et al., 2017). Mineral precipitation (i.e., calcite cementation and authigenic clay growth) can be seen as the process in which space is gradually occupied by minerals, whereas dissolution (i.e., feldspar or fragment dissolution) represents the opposite process. The variation in pore or mineral space can be used to describe the level of mineral precipitation and mineral dissolution on the pore space. Therefore, the precipitation level (r_c) and dissolution level (r_d) are given by:

$$r_p = \frac{\varphi_p}{\varphi_o} = \frac{\varphi_p}{\varphi_p + \varphi_m} \tag{3}$$

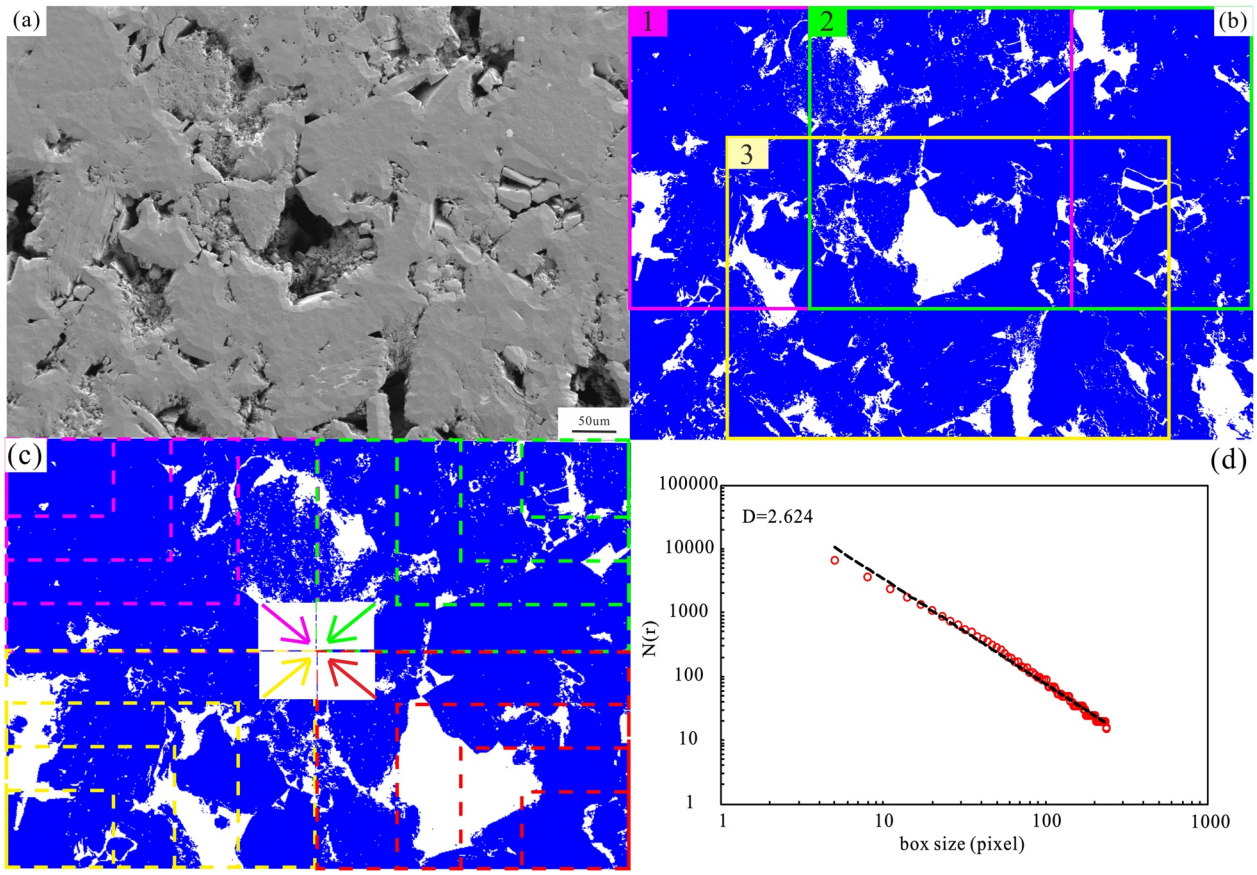

Figure 2. "Fractal dimension" calculation process based on scanning electron microscopy (SEM). The SEM image (a) was transformed into a binary image (b) using "Image J"; randomly three regions were selected in a binarized image (b), and the number of contour boxes under different box sizes were determined from four directions (c); the "fractal dimension" of sample S2 ("fractal dimension" D = 1-slope) is shown in part d as an example. The "fractal dimension" of the image was calculated using the "FracLac" module. Adapted from Zhou et al. (2020).

$$r_d = \frac{\varphi_d}{\varphi_m} = \frac{\varphi_m - \varphi_o}{\varphi_m} \tag{4}$$

where φ_o is the porosity before mineral precipitation or dissolution, %; φ_p is the porosity occupied by mineral precipitation, %; φ_d is the increasing porosity due to mineral precipitation, %; and φ_m is the porosity of the rocks, %. The value is negative for mineral precipitation processes and positive for mineral dissolution processes.

4. Results

The results of this study first examine the microscopic characteristics of the samples, through thin section description and SEM analysis, with particular focus on pore spaces, and contained diagenetic signals. From this, three reservoir types are defined (Type I, Type II, and Type III), based on diagenetic features. Recorded porosity, permeability, XRD mineral composition and NMR T_2 spectrum values of 13 samples are presented, and compared with their interpreted "reservoir types," in order to provide a link between observed diagenetic features, and associated parametrical recordings of reservoir quality.

4.1. Microscopic Analysis of Pore Space Character and Diagenetic Features

Thin section samples and SEM analysis show abundant diagenetic features in the Gaotaizi oil layer (sandstone reservoir), including mechanical compaction, pressure solution, rock fragment and feldspar dissolution, quartz overgrowth, calcite cementation/replacement, clay growth, and pyrite growth (Figure 3). The clearest evidence

Table 2
Analytical Results for the 13 Samples Analyzed in This Study, Including: Porosity and Permeability Information; Bulk-Rock XRD Analysis Results; and Carbonate Cementation Level (r_{ca}), Authigenic Clay Growth Level (R_{clay}), and Dissolution Level (r_d)

Well	Depth /m	Sample number	Porosity /%	Permeability /$\times10^{-3}\mu m^2$	Fractal dimension D	Quartz /%	Feldspar /%	Clay /%	Carbonate /%	Other /%	r_{ca}	r_{clay}	r_d
J191	1841.26	S1	15.35	1.1645	2.688	48.5	42.6	2.4	5.4	1.1	-	-	0.55
G72	2017.50	S2	18.03	15.8580	2.669	32.5	62.1	5.0	0.4	0.0	-	-	0.47
G921	1915.35	S3	10.95	1.1544	2.650	25.8	51.8	3.3	6.0	1.1	0.35	0.31	0.38
J44	2147.75	S4	9.40	0.9114	2.642	38.6	51.8	4.3	5.3	0.0	0.36	0.31	0.37
T234	1772.30	S5	16.26	1.8300	2.624	45.5	46.0	5.3	2.8	0.4	0.15	0.25	0.28
G708	2000.70	S6	6.71	0.0254	2.671	39.0	36.0	9.0	16.0	0.0	0.70	-	-
G93	2100.66	S7	12.61	0.1834	2.658	32.8	46.3	6.4	14.1	0.4	0.53	-	-
G921	1909.82	S8	6.62	0.0403	2.689	29.3	35.6	3.4	31.7	0.0	0.82	-	-
J191	1838.11	S9	11.90	0.1203	2.653	48.5	36.6	2.4	11.4	1.1	0.57	-	-
J393	1963.70	S10	9.94	0.0470	2.683	33.9	37.8	15.1	12.4	0.8	-	0.60	-
G931	2197.42	S11	6.75	0.0186	2.696	39.0	38.0	17.0	4.0	2.0	-	0.72	-
L23	1882.00	S12	16.60	0.0791	2.661	44.1	43.6	8.7	3.1	0.5	-	0.34	-
L29	1918.92	S13	14.46	0.0666	2.658	48.8	40.4	9.8	0.3	0.7	-	0.40	-

Note. Light gray rows represent samples from Type I reservoirs, light yellow rows from Type II reservoirs, and light blue from Type III reservoirs. More data references come from Krohn and Thompson (1986) and Krohn (1988) (Table 3). These samples include some well-known sandstone (i.e., Berea sandstone, Coconino sandstone and Table sandstone) and carbonate (Arab D, Austin Chalk, Bedford limestone, Smackover limestone and dolomite) as well as Blackhawk sandstones with various buried depth from well near Price River, Utah.

for diagenesis is the dissolution of rock fragments and feldspar (Figure 3a). Dissolution causes partial or complete removal of grains, resulting in the enlargement of pore space and increased complexity of the grain-pore interfaces. Quartz overgrowth is also observed (Figures 3a and 3b), but its area accounts for a low proportion within samples and therefore its influence on pore space character can be considered negligible.

Grain contact types tend to be point and line contact, with only a small number of line contact positions showing evidence for pressure solution, producing rough grain edges (Figures 3a and 3b). Mica grains are observed bent and deformed (Figure 3b), providing some additional evidence of the influence of compaction. Grain contact types, uncrushed mica and the similar burial depths of these sandstones (1772.30–2197.42 m in Table 2), indicates that the Gaotaizi oil layer (sandstone reservoir) experiences a same level of mechanical compaction, and the difference in porosity and permeability of the sandstone reservoir is not caused by anisotropic mechanical compaction.

The most significant diagenetic feature is calcite (Figure 3b), which fills the intergranular pores (and dissolved pores) in the form of a cement. Calcite occupies the pore space of feldspar grains in two ways, the first of which is through the dissolution of pore space followed by infilling of calcite cement (i.e., metasomatism). The morphological characteristics of the calcite cement depend on the original pore space characteristics caused by dissolution. The second mechanism is through mineral replacement of feldspar crystals, often resulting in the retention of the original feldspar crystal characteristics, such as double crystal form. In some examples, the intergranular pores are occupied by authigenic clay minerals, or pyrite (e.g., Figure 3c). Authigenic clay minerals and pyrite divide the intergranular pores into numerous smaller intercrystalline pores. The quantity of pyrite is comparatively small, and therefore its impact on the pore space is likely negligible.

The above observations show that dissolution, calcite cementation, and clay growth are the three principal diagenetic processes altering the pore space in the Gaotaizi oil layer; the effect of quartz overgrowth and pyrite growth on the pore spaces is thought to be low. On these bases, the reservoirs of the Gaotaizi oil layer are separated into three principal diagenetic processes types. First, Type I reservoirs where the intergranular pore size is further enlarged, mineral grain edges are partly dissolved, or even the entire grains are dissolved. Samples S1–S5 represent this type of reservoir (Table 2). Second, Type II reservoirs where the most important mineral affecting the pore space of the reservoir is calcite minerals. The intergranular pores are filled with calcite to varying levels, although part of the pores are also filled by clay minerals. Samples S6–S9 represent this type of reservoir (Table 2). Finally, Type III reservoirs where the intergranular pore space is affected by clay mineral growth, and only a small amount of other cement. Sample S10–S13 represent this type of reservoir (Table 2).

4.2. Reservoir Characterization—Porosity, Permeability, and Bulk-Rock Composition

Routine porosity and permeability measurements show that the physical properties of Gaotaizi oil layer (sandstone reservoirs) vary significantly, with porosity ranging from 6.62% to 18.03% and permeability ranging from 0.0186×10^{-3} to 15.8580×10^{-3} μm^2 (0.0188–16.0681 mD) (Table 2). The data shows that the porosities of Type I reservoirs, which range from 9.4% to 18.03%, are higher than that of Types II and III reservoirs that have porosity ranges from 6.71% to 12.61% and 6.75% to 14.46%, respectively. The permeabilities of Type I reservoirs ranges from 0.9114×10^{-3} to 15.8580×10^{-3} μm^2 (0.9235–16.0681 mD), which is higher than that of Type II reservoirs with values ranges from 0.0254×10^{-3} μm^2 (0.0257 mD) to 0.1824×10^{-3} μm^2 (0.1848 mD), and Type III reservoirs with values ranges from 0.0186×10^{-3} μm^2 (0.0188 mD) to 0.0791×10^{-3} μm^2 (0.0801 mD) (Figure 4a).

The bulk-rock XRD data (Table 2 and Figure 4) show that quartz and feldspar dominate in the Gaotaizi oil layer (sandstone reservoir), accounting for 29.3–48.5% and 35.6–62.1%, respectively. The carbonate and clay mineral content accounts for 0.3–31.7% and 2.4–17.0%, respectively (Table 2). Type I reservoirs have carbonate concentrations ranging between 0.4% and 6.0%, which are much lower than compared with Type II that have up to 31.7%. Similarly, Type I reservoirs have the lowest clay content ranging between 2.4% and 5.3%, with Type II reservoirs being slightly higher at 2.4–9.0%, and Type III reservoirs much higher 8.7–17% (Figure 4b).

The 13 sandstone samples were analyzed by NMR spectroscopy, with signal intensity plotted against "T_2" relaxation rate (Figure 5). The T_2 relaxation rate has a positive correlation with pore size, and the NMR signal intensity is closely related to the pore volume, therefore the NMR spectrum can be used to assess pore size distribution in reservoirs (Wang, Guan, et al., 2020). Figure 5 shows the NMR T_2 spectra of water-saturated samples, with the NMR signal ranging between 0.1 and 500 ms. The Type I reservoir (S1–S5) shows bimodal morphology, the left peak is mainly 0.1–10 ms, with peak values at approximately 2 ms, and the right peak varies from 10 to 500 ms, with peak values from 30 to 100 ms (Figure 5a). The NMR spectra of the other samples show a single peak or are single peak dominated, with peak varies from 0.1 to 10 ms and its values from 0.5 to 2 ms (Figures 5b and 5c).

4.3. Diagenetic Levels—Dissolution, Calcite Cementation, and Clay Growth

The major authigenic minerals are clay and carbonate, which serve as cement, and occupy the primary pore volume. Considering this, the primary pore volume can be divided into two parts: one part is the volume occupied by the carbonate or clay mineral, and the other part is the residual pore volume after carbonate cementation or clay growth, which can be measured and has been presented in Table 1. According to Equation 3, the carbonate cementation level (r_{ca}) and authigenic clay growth level (r_{clay}) can be expressed as the ratio of pore volume occupied by carbonate cement or authigenic clay to the original pore volume (i.e., the sum of measured porosity and porosity occupied by authigenic mineral).

For the reservoir that was dissolved with various levels (Type I reservoir), it is difficult to determine the original mineral content within the pore spaces. Therefore, additional quantitative control is required in order to study the impact of dissolution on pore space; NMR analysis can provide an important insight into pore space character. In most examples, the pore and grain sizes in sandstones are often log-normally dispersed, at least over much

Table 3
Fractal Dimension of Sandstone and Carbonate Rocks From Published Literature (Krohn, 1988; Krohn & Thompson, 1986)

Sample	Porosity%	Permeability (mD)	Fractal dimension D
Berea sandstone	20	123	2.85
Coconino sandstone	9.9	0.037	2.75
Table sandstone	35	4,933	2.55
Blackhawk sandstones from well near Price River, Utah			
41.8 m (137.3 ft)	11.7	1.84	2.60
47.2 m (154.8 ft)	4.3	0.022	2.59
49.3 m (161.7 ft)	11.5	21.7	2.66
51.6 m (169.3 ft)	14..	13.6	2.72
68.5 m (224.8 ft)	7.5	0.02	2.73
Arab D	–	–	2.27
Austin Chalk	–	–	2.59
Bedford Limestone	–	–	2.35
Smackover Limestone	–	–	2.65
Smackover Dolomite	–	–	2.75

of the size range (Beaucage et al., 2004; Burger, 1976), and any multimodal distribution of pore size is typically associated with diagenesis (Emmanuel & Berkowitz, 2007).

Thin section analysis shows that sandstone samples S1–S5 (Type I reservoirs) are all significantly dissolved (Figure 3a). Interestingly, the NMR spectra of those samples forms a bimodal morphology (Figure 5). The left peak of the bimodal NMR spectrum is considered to be the pore size distribution formed by the mechanical compaction of deposited grains, and the right peak can be related to the dissolution of feldspar and rock fragments. Therefore, the pore volume of sandstones before dissolution occurs can be represented by the area enclosed by the left peak using logarithm Gaussian fitting and the abscissa, and the increased pore volume by dissolution can be calculated by the difference value of the NMR area and the area of left peak. on these bases, the dissolution level of type I reservoir could be calculated by Equation 4, and Figure 6 schematically shows the calculation process of a sandstone sample.

The calculated dissolution level of Type I reservoir ranges from 0.28 to 0.55, the carbonate cementation level of Type II reservoir ranges from 0.53 to 0.82, and the clay growth level of Type III reservoir ranges from 0.34 to 0.72. Since the levels of mineral precipitation, such as calcite cementation and clay growth, in the selected samples is generally high, samples S3–S5, with low levels of mineral dissolution, are also used to calculate the levels of calcite cementation and clay growth, representing the cases of a low levels of mineral precipitation.

4.4. Fractal Pore Structure Characteristic

In the Gaotaizi oil layer, two samples (samples S4 and S5 in this study, with "fractal dimensions" $D = 2.64$ and 2.62) are chosen to illustrate the impact of primary sedimentary deposit configuration on fractal behavior. The thin sections show similar diagenetic characteristics; parts of the grains are dissolved, while the dissolution level is low ($r_d = 0.37$ in sample S4 and $r_d = 0.28$ in sample S4, respectively), and small amounts of cement are present within intergranular pores and intergranular dissolved pores. However, the grain size and roundness of these two samples are variable, the main grain size distribution of sample S4 ranges from 100 to 200 μm (Figure 7a), which is larger than that of sample S5, whose grain sizes is distributed in the range of 50–100 μm (Figure 7b). Moreover, the thin section also shows that the grain edges of sample S4 are more tortuous than those of sample S5 (Figure 7). A similar phenomenon is observed through the SEM analysis for unpolished sample, with the initial grain surface morphology in sample S4 being rougher than that of sample S5; the initial deposited grain surface morphology (nondissolved grain surface) of sample S4 is fluctuating (Figure 8a), while the initial deposited grain surface of sample S5 is flat (Figure 8b). These observations indicate that that the roughness of the initial grain-pore interface is controlled (to some extent) by the grain size of the sedimentary rocks. For example, finer grain sizes tend to have more spherical/round grains, which produce smoother grain-pore interfaces, resulting in a lower "fractal dimension."

Figure 9a shows that the "fractal dimension" increases with cementation level, and clay growth has a greater impact on the "fractal dimension" of rock than carbonate cementation. Moreover, the pore space configuration, characterized by the SEM analysis for unpolished surface, also illustrates that calcite cementation and clay growth will reduce the pore size and increase the roughness of the grain-pore interface (Figures 8c and 8d). More favorable evidence is given in Figure 2 of Aharonov et al. (1997), which shows that the "fractal dimension" (see the Coconino, Table and Blackhawk sandstones (49.3 m) in Table 3 in this study) increases with increasing alteration of the initial grains and precipitation of pore-lining minerals. Figure 9b also shows that the "fractal dimension" increases with dissolution level, which indicates that the roughness of the grain–pore interface increases with the level of mineral dissolution. The SEM analysis for unpolished surface of sample S2 shows that the grain-pore interface becomes rougher after being dissolved (Figure 8e), moreover, dissolution makes the edges of the grain more tortuous (Figure 3a).

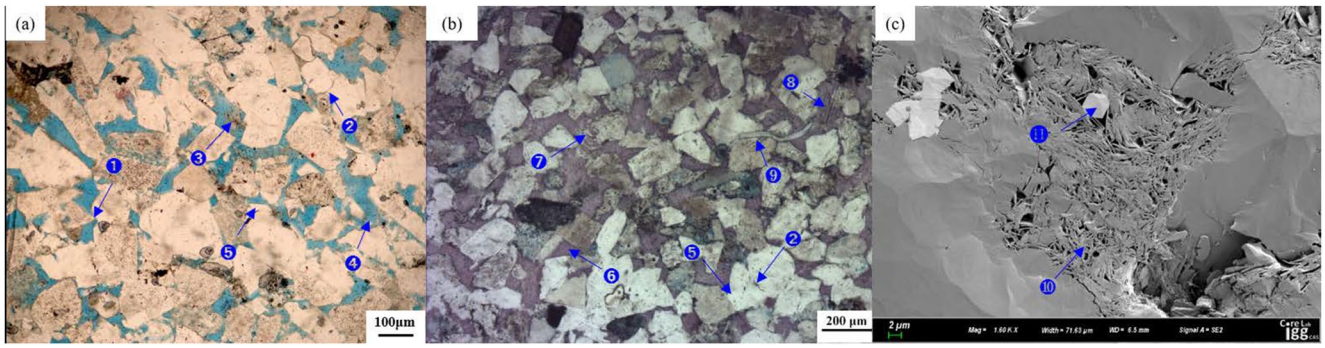

Figure 3. Thin section and scanning electron microscopy (SEM) images, illustrating three principal diagenetic processes altering the pore space in the Gaotaizi oil reservoir. (a) Sample S2, (b) S8, and (c) S11 represent the reservoir mainly affected by dissolution, carbonate cementation, and clay growth, respectively. ❶ Mechanical compaction, point-contact type between grains; ❷ Pressure solution, line contact type between grains; ❸ Rocks fragment dissolution. Most of the rocks fragment grain is dissolved, leaving only a small amount of residual parts; ❹ Feldspar dissolution. Part of the edges of feldspar grains are dissolved, and the sedimentary morphology of the grains can be easily identified; ❺ Quartz overgrowth. The thickness of the quartz overgrowth is about 20–30 μm; ❻ Calcite cementation. Calcite fills the intergranular pores; ❼ Calcite cementation. Calcite fills the dissolved pore caused by feldspar dissolution; ❽ Metasomatism. The feldspar grains are replaced by calcite and the feldspar polysynthetic twin structure remains; ❾ Mechanical compaction. Mica is bent and deformed due to compaction; ❿ Clay growth. Authigenic illite clay mineral serves as cement to fill the intergranular pores and divides the intergranular pores into numerous tiny clay intercrystalline pores; ⓫ Pyrite growth. A single crystal of pyrite grows in the middle of the clay minerals.

5. Discussion

The initial pore space configuration, such as pore size distribution and grain-pore interface morphology, depends on the characteristics of primary sedimentary grains, including mineral type grain size, sorting, rounding and packing (Ehlers & Blatt, 1982; Reineck & Singh, 1980). During progressively more-protracted transportation processes, unstable components (i.e., feldspar and rock fragments) gradually decrease in size, matrix grain size gradually decrease, and the roundness gradually improves (Zhu, 2008). In a very general sense, small grain sizes imply they were likely transported further, with high roundness and smooth surfaces. These sediment construct relatively narrow and smooth pore systems, leading to a low value of the fractal upper limit, and a lower "fractal dimension." The "fractal dimension" and grain-pore surface morphology of sample S4 and sample S5 demonstrate that "fractal dimension" or the roughness of the initial grain-pore interface decrease with the deposited grain size (Figures 7a, 7b and 8a, 8b). In the sandstone reservoir of the Gaotaizi oil layer, the provenance is from the north (Figure 1), with sediments transported by rivers to the delta front in which they are deposited and preserved. Therefore, the "fractal dimension" of sample S5, which is further away from the sedimentary provenance, with smaller deposited grains sizes and higher roundness, is more-comparable with sample S4. Moreover, the value of the fractal upper limit depends on the pore space characteristics constituting by the sedimentary grains, while fractal lower limit is limited by the individual grain size diameter of 2 nm (Katz & Thompson, 1985).

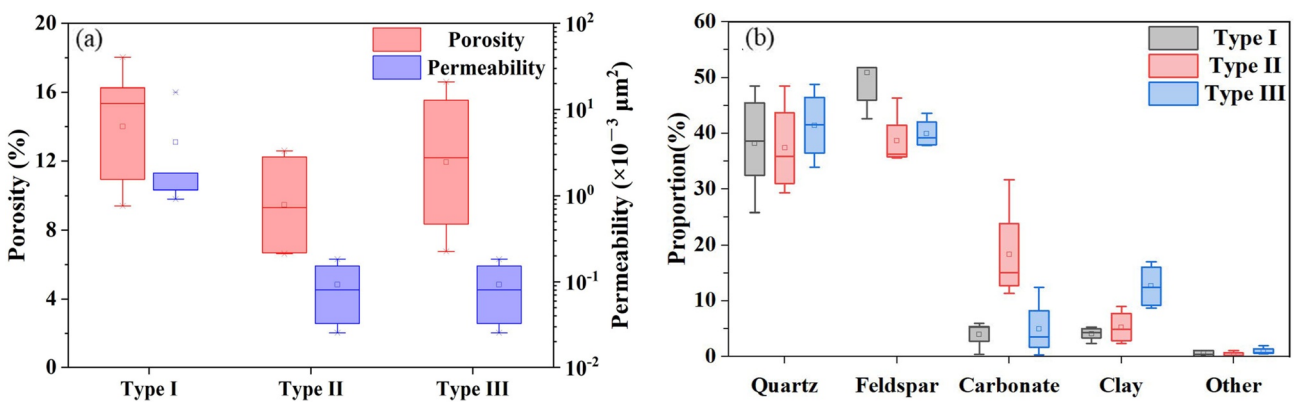

Figure 4. Graphical plots of the porosity, permeability, and mineral content in the three reservoir types. (a) Comparison of porosity and permeability between different reservoir types. (b) Plot of bulk-rock X-ray diffraction analysis (XRD) results, showing a comparison of mineral concentrations in the Type I, Type II, and Type III reservoirs.

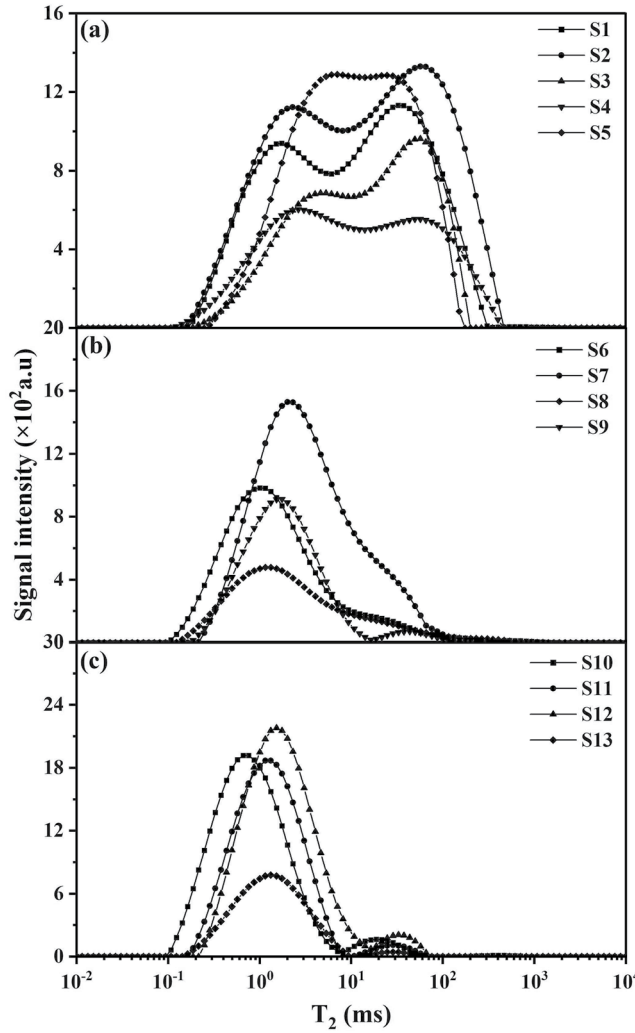

Figure 5. Nuclear magnetic resonance spectrum of 13 samples. The nuclear magnetic resonance (NMR) spectra of Type I samples (S1–S5) show a bimodal profile (a), while Type II (S6–S9) (b) and Type III (S10–S13), (c) reservoir sandstones display either a single peak, or a single peak dominated profile.

Two schematic diagrams are provided that demonstrate the impact of sedimentation on the pore system. Figures 10a and 10c are two types (end member models) of pore system, consisting of a range of sedimentary grains. In the first model (Figure 10a), the deposited grains are larger with higher roundness, giving the sample a wider (larger) pore space, with rougher grain-pore interfaces. In comparison, the second model (Figure 10c) shows smaller pore spaces, with smoother grain-pore interfaces.

The pore space configuration formed by the primary sedimentary deposit will be further altered by mechanical compaction (Athy, 1930; Guo et al., 2013) and chemical diagenesis (Ehlers & Blatt, 1982; Emmanuel et al., 2015; Stack, 2015). The mechanical compaction process can be considered as a continuation of the deposition process, which alters the pore space by developing overburden. This process will reduce the pore size, resulting in a decreasing of "fractal upper limit," and lead to a relative increase in the roughness of the grain-pore interface, thereby increasing the "fractal dimension." The data for Blackhawk sandstones (Table 3) provides additional evidence to illustrate the impact of mechanical compaction on fractal behavior, and that "fractal dimension" increases with burial depths. It should be noted that present day burial depth does not always reflect the level of mechanical compaction, because it may be the result of the uplift of the stratigraphic.

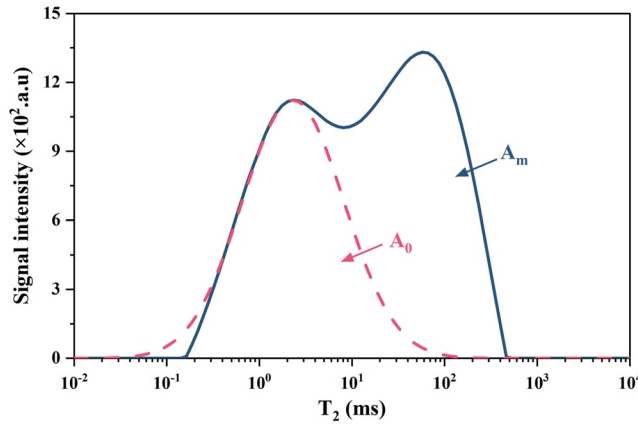

Figure 6. Schematic diagram of the calculation process of dissolution level. The solid line is the nuclear magnetic resonance (NMR) spectrum of sample S2 with water saturation. The dotted line is the distribution of the front peak of the nuclear magnetic field using logarithmic Gaussian fitting. A_m is an area enclosed by the solid line and the abscissa. A_0 is an area enclosed by the dotted line and the abscissa. Dissolution level = $(A_m - A_0)/A_m$.

After rocks undergo mechanical compaction, chemical diagenesis can further alter the fractal pore structure (Aharonov et al., 1997). Figure 9 shows that "fractal dimension" increases with more-advanced alteration of initial grains and/or precipitation or dissolution of the pore-lining minerals. In the process of mineral precipitation, crystal growth on grain-pore interfaces result in a narrowing of the pore space, causing the fluids to spend more time in the pore, and thus become more chemically equilibrated with the surrounding solid. Therefore, the number of ions leaving the interface gradually approaches the number attaching to it during the cementation, which is equivalent to $p\_/p_+ \rightarrow 1$ as per Aharonov and Rothman's (1996) model. This process tends to narrow the pore size, roughen grain-pore interface and complicates the pore system, leading to a low value of the fractal upper limit and a high value of the "fractal dimension." However, calcite cementation and clay growth have different effects on the fractal lower limit. Since the surface tension is negative, clays like to maximize their surface area on all possible length scales, which would lead to the fractal surfaces of clays extending from a few angstroms to a few microns (Wong et al., 1986).

Figures 10c and 10d show (schematically) the alteration of pore structure of rock by mineral precipitation. A cementation (clay growth) occurs, and progresses the narrow channel between pore H and G disappears (Figure 10c) and then becomes divided into multiple separate pores through clay minerals growth (Figure 10d). In this example, Pore I is completely cemented, while pore F is only cemented on the surface by carbonate minerals.

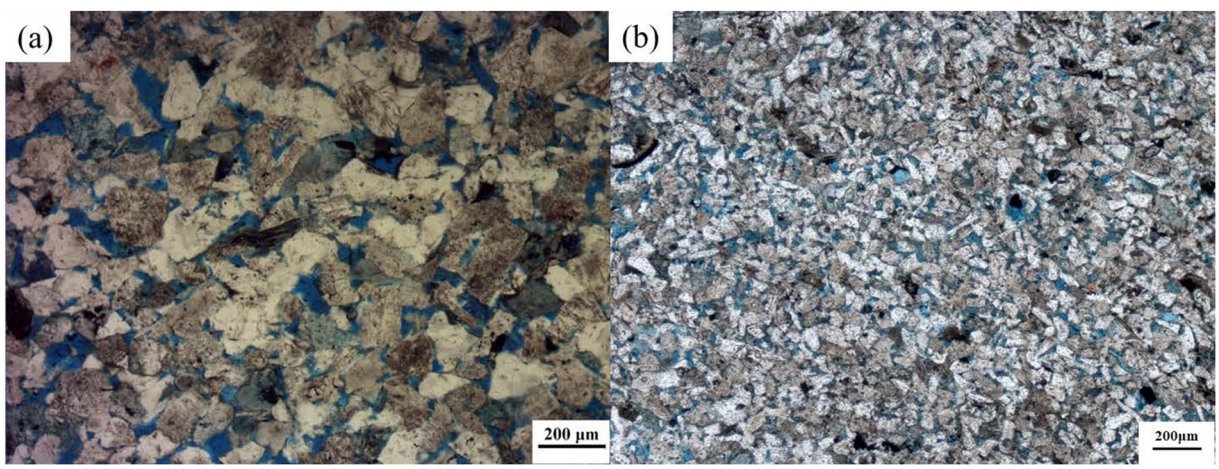

Figure 7. Thin section images demonstrating the impact of primary sedimentary deposit configuration on pore structure. The size of the deposited grains in sample S4 (a) are larger, and the roundness is lower, than in sample S5 (b).

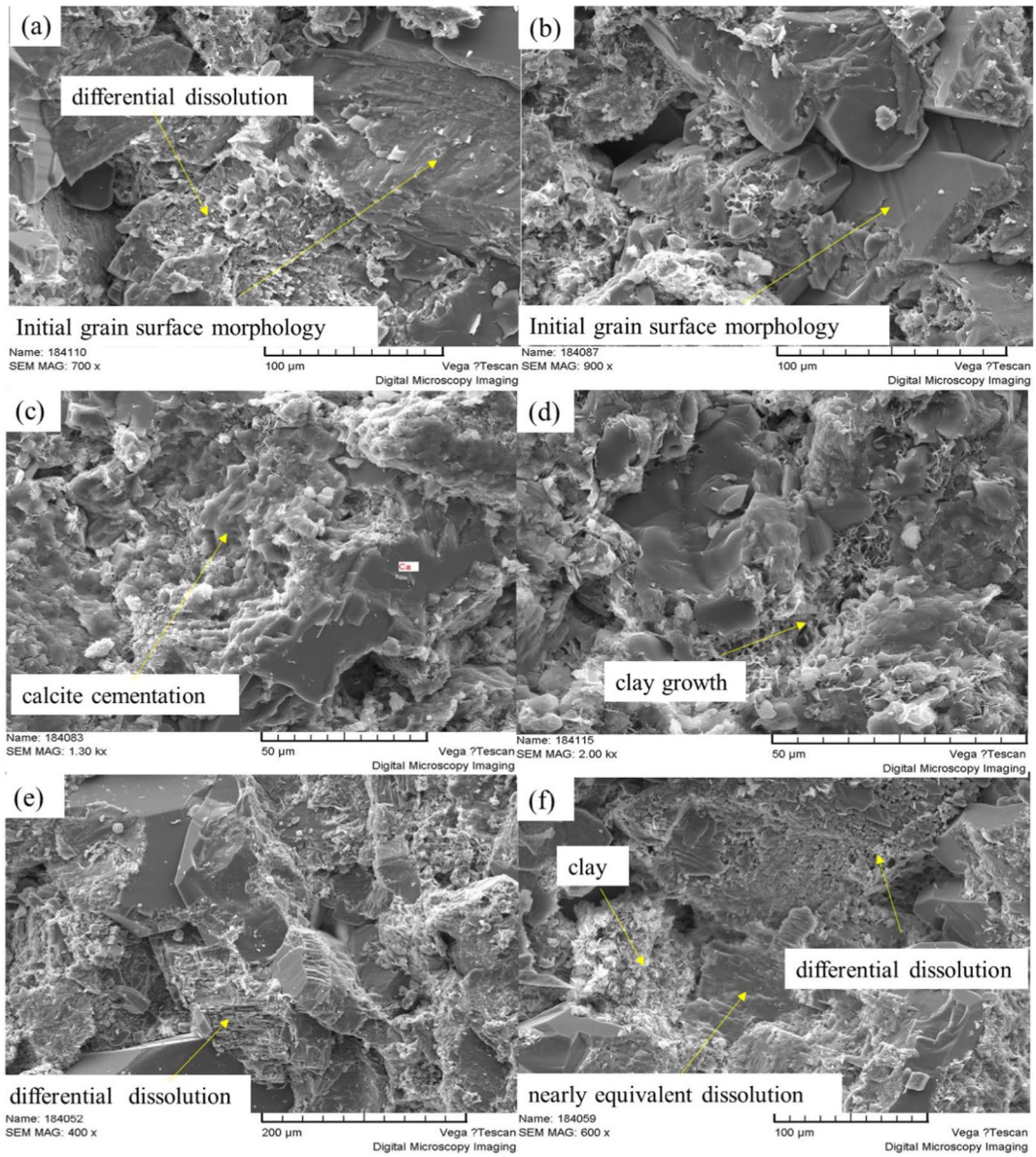

Figure 8. Influence of geological processes on rock surface morphology, as illustrated in images of unpolished surface. (a, b) Initial grain surface morphology of different grain sizes. The grain size of sample S4 (a) is larger than that of sample S5 (b). (c) Sample S9: surface morphology of calcite cementation. (d) Sample S10: surface morphology of clay growth. (e, f) Sample S2: surface morphology of grain after differential dissolution (e) and nearly equivalent dissolution (f).

Crystal growth and dissolution on the grain-pore interface is a competitive process driven by mineral deposition and dissolution (Emmanuel et al., 2010). Theoretically, if every position on the interface is dissolved equally, that is, the reverse process of cementation, the "fractal dimension" will decrease with a decrease of relative roughness of the grain-pore interface and the fractal upper limit will increase with an increase of pore size (Figure 8f). However, the chemical reactions rate between different minerals and formation fluids are quite various (Beckingham et al., 2017)—as is often the case in geological systems—i.e., feldspar tends to be dissolved while quartz exhibit insoluble feature. Feldspars, which are typically larger than compared with the rest of the matrix grains, can form large pits or holes when they are dissolved, with rough grain-pore interfaces (Figures 1a and 8e, 8f). In summary, dissolution tends to widen the pore size, roughens the surface and thereby increases the "fractal dimension" and "fractal upper limit."

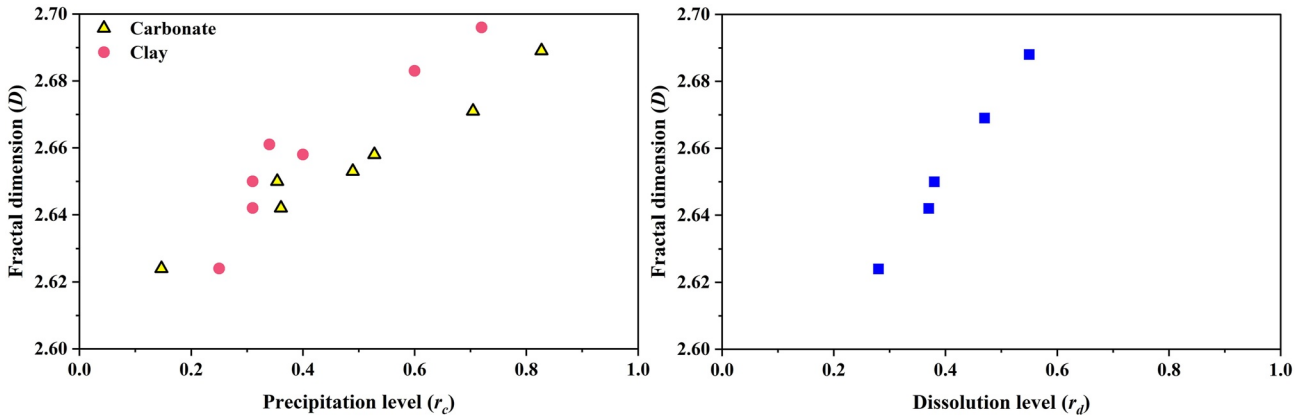

Figure 9. Measured "fractal dimension" versus precipitation (a) and dissolution level (b). Plots show a linear increase of "fractal dimension" with precipitation and dissolution level.

The schematic diagrams of Figures 10b and 10d illustrate a generalized pore space evolution with dissolution, where: Pore E is isolated after dissolution; a new conduit forms between pores B and D due to surface dissolution; and pores A and C form a connection through grain dissolution. At the same time, differential dissolution results in some grains becoming severely dissolved to form complex surfaces, while other minerals are dissolved slightly in the interface.

Sedimentation and subsequent lithification (rock formation) is an extremely complex process that combines multiple physical and chemical reactions. Studying geological processes using single proxy-approaches, such as sedimentology, or analysis of cementation/dissolution, is insufficient to describe the evolution of fractal properties on the grain-pore interface. Every process has an impact on fractal behavior in various geological history periods, and the experimental fractal properties are the final consequence of multiple geological processes. This study provides an important analysis of the mechanism of the main geological processes (sedimentation, mechanical compaction, cementation, and dissolution) on fractal behavior.

However, the mechanism and influence of other geological processes (such as pressure solution, recrystallization, and surface diffusion) on fractal behavior are not shown in the schematic. Since the main geological processes mask the effects of the other processes on fractal behavior, it is difficult to identify the corresponding geological feature within the samples for experimental support. Since the fractal pore structure is closely related to the grain-pore interface, and the evolution of grain-pore interface with chemical diagenesis can be described by the interface growth equation (Aharonov & Rothman, 1996; Kardar et al., 1986):

$$\frac{\partial h}{\partial t} = \lambda\left(1 + \frac{1}{2}(\nabla h)^2\right) + v\nabla^2 h + \eta(x,t) \tag{5}$$

The first part describes the evolution of surface height "h" that all sites on the interface grow with equal probability and interface growth velocity "λ," in the direction normal to the local surface orientation (Aharonov & Rothman, 1996). This process can be regarded as both the calcite cementation (Figure 8c) and the equal dissolution processes (Figure 8f). The second part describes an evolution of interface height due to smoothing mechanisms, such as surface tension effects, surface diffusion, mechanical erosion, weathering, and recrystallization, which result in an effective diffusion coefficient "v." Commonly, the diffusion process will rearrange the solid phase beneath the interface, resulting in a flat surface (Carrier & Pearson, 1988). Some carbonate rocks growing in clean water with a low "fractal dimension," such as Arab D and Bedford limestone (Krohn, 1988, Table 3), may be attributed to the effect of surface tension. In the growth of mineral, the surface roughness is determined by the competition between the thermal fluctuations and the surface tension if the water is clean (Wong et al., 1986). The growth of these limestones is at a low temperature; thus, the surface tension dominates the surface roughness. The third part reflects fluctuations ("η") in geological processes such as crystallization position and crystal growth anisotropy. If the pore water contains ions such as Mn^{2+} and Fe^{2+}, these ions randomly occupy the surface of the rock and typically lower the surface tension, which makes the pore space more complicated. This may be why high "fractal dimension" values are also observed in carbonate rocks, such as Austin Chalk, Smackover limestone

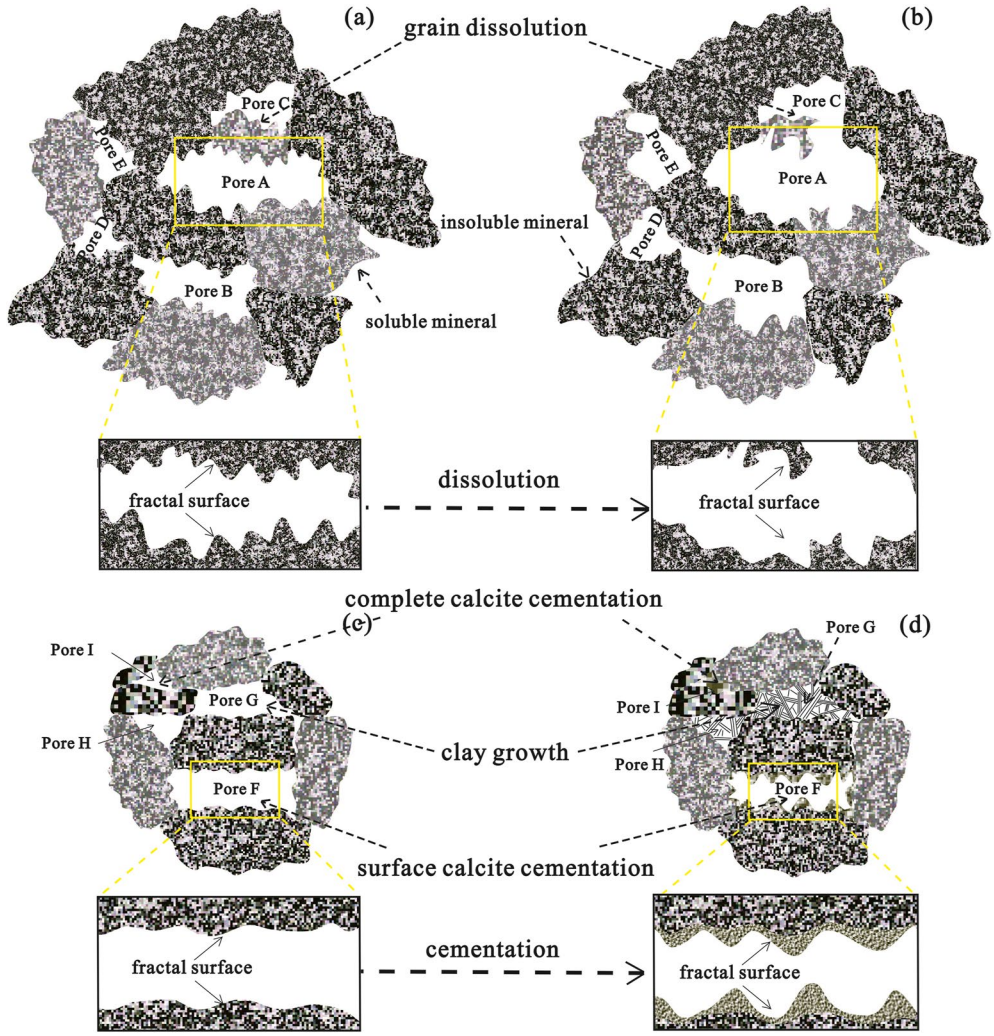

Figure 10. Schematic diagram of the impact of sedimentation, dissolution, and cementation on the grain-pore interface in sedimentary rocks. (a) Pore system consists of large grains, with a rough surface; (b) Pore system evolves form (a) though dissolution; (c) Pore system consists of small grains, with smooth surfaces; (d) Pore system evolves by calcite cementation and clay growth from (a); (a, c) are contrasted to illustrate the effect of sedimentation on the grain-pore interface in sedimentary rocks, (a, b) are contrasted to illustrate the effect of dissolution the grain-pore interface in sedimentary rocks, and (c, d) are contrasted to illustrate the effect of cementation on the grain-pore interface in sedimentary rocks.

and dolomite (Krohn, 1988, Table 3). However, in the evolution process of the pore space by the second and third part, the grain-pore interface does not strictly follow the power law dependence for pore size and the surface height "*h*" (Equation 1), thereby exhibiting nonfractal behavior (Aharonov & Rothman, 1996). Therefore, these two processes will lead to a lower value of the "fractal upper limit."

6. Conclusions

The initial pore configuration formed by sedimentary grains tends to exhibit fractal behavior, its "fractal dimension" and fractal upper and low limit depend on the pore structure, constituted by deposited grain characteristics and surface morphology. Diagenesis alters the initial fractal pore structure over time. The mechanical compaction process reduces the pore space, resulting in a relative increase in the "roughness" amplitude of the pore-grain interface, this process decreases the fractal upper limit and increases the value of the "fractal dimension." Dissolution, cementation and random fluctuations will increase the roughness of the interface, resulting in a high "fractal dimension." Moreover, dissolution will increase the fractal upper limit, while other types of diagenesis

will lower the fractal upper limit. The fractal lower limit is indicated by the grain size, but it will decrease as the clay grows. The fractal behavior exhibited by sedimentary rock is the cumulative consequence of multiple geological processes, which need to be properly understood in order to more-accurately predict reservoir quality in the subsurface.

Data Availability Statement

The experimental test data used for supporting the finding in the study are available at MS-Date via https://doi.org/10.6084/m9.figshare.17169227.v1 in figshare website with Katz and Thompson (1985) and Krohn (1988).

Acknowledgments
This work was supported by the National Natural Science Foundation of China (41922015) and National Science and Technology major projects (2016ZX05046-001-005). The paper is published by permission of the Executive Director, British Geological Survey (UKRI).

References

Aharonov, E., & Rothman, D. H. (1996). Growth of correlated pore-scale structures in sedimentary rocks: A dynamical model. *Journal of Geophysical Research*, *101*, 2973–2987. https://doi.org/10.1029/95JB03209

Aharonov, E., Rothman, D. H., & Thompson, A. H. (1997). Transport properties and diagenesis in sedimentary rocks: The role of micro-scale geometry. *Geology*, *25*, 547–550. https://doi.org/10.1130/0091-7613(1997)025<0547:TPADIS>2.3.CO;2

Ai, T., Zhang, R., Zhou, H. W., & Pei, J. L. (2014). Box-counting methods to directly estimate the fractal dimension of a rock surface. *Applied Surface Science*, *314*, 610–621. https://doi.org/10.1016/j.apsusc.2014.06.152

Anovitz, L. M., Cole, D. R., Jackson, A. J., Rother, G., Littrell, K. C., Allard, L. F., et al. (2015). Effect of quartz overgrowth precipitation on the multiscale porosity of sandstone: A (U)SANS and imaging analysis. *Geochimica et Cosmochimica Acta*, *153*, 199–222. https://doi.org/10.1016/j.gca.2015.01.028

Anovitz, L. M., Cole, D. R., Rother, G., Allard, L. F., Jackson, A. J., & Littrell, K. C. (2013). Diagenetic changes in macro- to nano-scale porosity in the St. Peter Sandstone: An (ultra) small angle neutron scattering and backscattered electron imaging analysis. *Geochimica et Cosmochimica Acta*, *102*, 280–305. https://doi.org/10.1016/j.gca.2012.07.035

Athy, L. F. (1930). Density, porosity and compaction of sedimentary rock. *AAPG Bulletin*, *14*, 1–24. https://doi.org/10.1306/3D93289E-16B1-11D7-8645000102C1856D

Avnir, D., Farin, D., & Pfeifer, P. (1984). Molecular fractal surfaces. *Nature*, *308*, 261–263. https://doi.org/10.1038/308261a0

Beaucage, G., Kammler, H. K., & Pratsinis, S. E. (2004). Particle size distributions from small-angle scattering using global scattering functions. *Journal of Applied Crystallography*, *37*, 523–535. https://doi.org/10.1107/S0021889804008969

Beckingham, L. E., Steefel, C. I., Swift, A. M., Voltolini, M., Yang, L., Anovitz, L. M., et al. (2017). Evaluation of accessible mineral surface areas for improved prediction of mineral reaction rates in porous media. *Geochimica et Cosmochimica Acta*, *205*, 31–49. https://doi.org/10.1016/j.gca.2017.02.006

Bi, H., Li, J., Tang, Z., Li, P., Wang, L., & Shang, X. (2017). High-resolution sequence stratigraphy, sedimentology and reservoir quality evaluation of the Yaojia Formation in the Longxi area of the Western Slope, Songliao Basin, China. *Marine and Petroleum Geology*, *88*, 511–530. https://doi.org/10.1016/j.marpetgeo.2017.09.004

Burger, H. (1976). Log-normal interpolation in grain size analysis. *Sedimentology*, *23*, 395–405. https://doi.org/10.1111/j.1365-3091.1976.tb00057.x

Cai, J., Zhang, Z., Wei, W., Guo, D., Li, S., & Zhao, P. (2019). The critical factors for permeability-formation factor relation in reservoir rocks: Pore-throat ratio, tortuosity and connectivity. *Energy*, *188*, 116051. https://doi.org/10.1016/j.energy.2019.116051

Carrier, G. F., & Pearson, C. E. (1988). *Partial differential equations: Theory and technique*. Academic Press. https://doi.org/10.1088/0031-9112/28/3/053

Chen, F., Lu, S., & Ding, X. (2014). Evaluation on hydrocarbon-generation amount of middle-shallow source rocks of Qijia-Gulong depression in Songliao Basin. *Aata Sedimentologica Sinica*, *32*, 1181–1187. https://doi.org/10.14027/j.cnki.cjxb.2014.06.020

Chen, X., & Yao, G. (2017). An improved model for permeability estimation in low permeable porous media based on fractal geometry and modified Hagen-Poiseuille flow. *Fuel*, *210*, 748–757. https://doi.org/10.1016/j.fuel.2017.08.101

Cihan, A., Tyner, J. S., & Perfect, E. (2009). Predicting relative permeability from water retention: A direct approach based on fractal geometry. *Water Resources Research*, *45*, W04404. https://doi.org/10.1029/2008WR007038

Costa, A. (2006). Permeability-porosity relationship: A reexamination of the Kozeny-carman equation based on a fractal pore-space geometry assumption. *Geophysical Research Letters*, *33*, L02318. https://doi.org/10.1029/2005GL025134

Daigle, H., Johnson, A., & Thomas, B. (2014). Determining fractal dimension from nuclear magnetic resonance data in rocks with internal magnetic field gradients. *Geophysics*, *79*, 425–D431. https://doi.org/10.1190/geo2014-0325.1

Ehlers, E. G., & Blatt, H. (1982). *Petrology: Igneous, sedimentary, and metamorphic*. W.H. Freeman and Company.

Emmanuel, S., Ague, J. J., & Walderhaug, O. (2010). Interfacial energy effects and the evolution of pore size distributions during quartz precipitation in sandstone. *Geochimica et Cosmochimica Acta*, *74*, 3539–3552. https://doi.org/10.1016/j.gca.2010.03.019

Emmanuel, S., Anovitz, L. M., & Day-Stirrat, R. J. (2015). Effects of coupled chemo-mechanical processes on the evolution of pore-size distributions in geological Media. *Reviews in Mineralogy and Geochemistry*, *80*, 45–60. https://doi.org/10.2138/rmg.2015.03

Emmanuel, S., & Berkowitz, B. (2007). Effects of pore-size controlled solubility on reactive transport in heterogeneous rock. *Geophysical Research Letter*, *34*, 125–141. https://doi.org/10.1029/2006GL028962

Feng, Z., Fang, W., Li, Z., Wang, X., Huo, Q., Huang, M., et al. (2011). Depositional environment of terrestrial petroleum source rocks and geochemical indicators in the Songliao Basin. *Science China (Earth Sciences)*, *54*, 1304–1317. https://doi.org/10.1007/s11430-011-4268-0

Feng, Z. H., Fang, W., Wang, X., Huang, C. Y., Huo, Q. L., Zhang, J. H., et al. (2009). Microfossils and molecular records in oil shales of the Songliao Basin and implications for paleo-depositional environment. *Science in China Series D—Earth Sciences*, *52*, 1559–1571. https://doi.org/10.1007/s11430-009-0121

Guo, Q., Chen, X., Song, H., Zheng, M., Huang, J., Chen, N., & Gao, R. (2013). Evolution and models of shale porosity during burial process. *Natural Gas Geoscience*, *24*, 439–449.

Issa, M. A., Issa, M. A., Islam, M. S., & Chudnovsky, A. (2003). Fractal dimension—A measure of fracture roughness and toughness of concrete. *Engineering Fracture Mechanics*, *70*, 125–137. https://doi.org/10.1016/S0013-7944(02)00019-X

Kardar, M., Parisi, G., & Zhang, Y. C. (1986). Dynamic scaling of growing interfaces. *Physical Review Letters*, *56*, 889–892. https://doi.org/10.1103/PhysRevLett.56.889

Katz, A. J., & Thompson, A. H. (1985). Fractal sandstone pores: Implications for conductivity and pore formation. *Physical Review Letters*, *54*, 1325–1328. https://doi.org/10.1103/PhysRevLett.54.1325

Krohn, C. E. (1988). Fractal measurements of sandstones, shales, and carbonates. *Journal of Geophysical Research*, *93*, 3297–3305. https://doi.org/10.1029/JB093iB04p03297

Krohn, C. E., & Thompson, A. H. (1986). Fractal sandstone pores: Automated measurements using scanning-electron-microscope images. *Physical Review B*, *33*, 6366. https://doi.org/10.1103/PhysRevB.33.6366

Li, K., & Horne, R. N. (2006). Comparison of methods to calculate relative permeability from capillary pressure in consolidated water-wet porous media. *Water Resources Research*, *420*, 285–293. https://doi.org/10.1029/2005WR004482

Liu, Y. (2007). A fractal model for relative permeability of unsaturated porous media with capillary pressure effect. *Fractals*, *15*, 217–222. https://doi.org/10.1142/S0218348X07003617

Lu, S., Li, J., Zhang, P., Xue, H., Wang, G. L., Zhang, J., & Li, Z. (2018). Classification of microscopic pore-throats and the grading evaluation on shale oil reservoirs. *Petroleum Exploration and Development*, *45*, 436–444. https://doi.org/10.1016/S1876-3804(18)30050-8

Lu, S., Xue, H., Wang, M., Xiao, D., Huang, W., Li, J., et al. (2016). Several key issues and research trends in evaluation of shale oil. *Acta Petrolei Sinica*, *37*, 1309–1322.

Moulu, J. C., Vizika, O., Kalaydjian, F., & Duquerroix, J. P. (1997). A new model for three-phase relative permeabilities based on a fractal representation of the porous media. *Paper presented at SPE Annual Technical Conference and Exhibition, San Antonio, TX, USA (SPE 38891)*. https://doi.org/10.2118/38891-MS

Nigon, B., Englert, A., Pascal, C., & Saintot, A. (2017). Multiscale characterization of Joint surface roughness. *Journal of Geophysical Research: Solid Earth*, *122*, 9714–9728. https://doi.org/10.1002/2017JB014322

Power, W. L., & Tullis, T. E. (1991). Euclidean and fractal models for the description of rock surface roughness. *Journal of Geophysical Research*, *96*, 415–424. https://doi.org/10.1029/90JB02107

Qiao, J., Zeng, J., Jiang, S., & Wang, Y. (2020). Impacts of sedimentology and diagenesis on pore structure and reservoir quality in tight oil sandstone reservoirs: Implications for macroscopic and microscopic heterogeneities. *Marine and Petroleum Geology*, *111*, 279–300. https://doi.org/10.1016/j.marpetgeo.2019.08.008

Rahner, S. M., Matthias, H., Celso, P. F., Andreas, W., & Viviane, S. (2018). Fractal dimensions of pore spaces in unconventional reservoir rocks using X-ray nano- and micro-computed tomography. *Journal of Natural Gas Science and Engineering*, *55*, 298–311. https://doi.org/10.1016/j.jngse.2018.05.011

Reineck, H. E., & Singh, I. B. (1980). *Depositional sedimentary environments-with reference to terrigenous clastics* (2nd ed., p. 549). Springer-Verlag.

Roy, A., Perfect, E., Dunne, W. M., & McKay, L. D. (2007). Fractal characterization of fracture networks: An improved box-counting technique. *Journal of Geophysical Research*, *112*, B12201. https://doi.org/10.1029/2006JB004582

Shi, L., Wang, Z., Zhang, Y., Zhang, G., & Xing, E. (2015). Distribution and formation of tight oil in Qijia area, Songliao Basin, NE China: *Petroleum exploration and development*, *42*, 48–55. https://doi.org/10.1016/S1876-3804(15)60005-2

Stack, A. G. (2015). Precipitation in pores: A geochemical frontier. *Reviews in Mineralogy and Geochemistry*, *80*, 165–190. https://doi.org/10.2138/rmg.2015.80.05

Thompson, A. (1991). Fractals in rock physics. *Annual Reviews earth planet science*, *19*, 237–262. https://doi.org/10.1146/annurev.ea.19.050191.001321

Thompson, A. H., Katz, A. J., & Krohn, C. E. (1987). The microgeometry and transport properties of sedimentary rock. *Advances in Physics*, *36*, 625–694. https://doi.org/10.1080/00018738700101062

Vadapalli, U., Srivastava, R. P., Vedanti, N., & Dimri, V. P. (2014). Estimation of permeability of a sandstone reservoir by a fractal and Monte Carlo simulation approach: A case study. *Nonlinear Processes in Geophysics*, *21*, 9–18. https://doi.org/10.5194/npg-21-9-2014

Wang, H., Liu, Y., Song, Y., Zhao, Y., Zhao, J., & Wang, D. (2012). Fractal analysis and its impact factors on pore structure of artificial cores based on the images obtained using magnetic resonance imaging. *Journal of Applied Geophysics*, *86*, 70–81. https://doi.org/10.1016/j.jappgeo.2012.07.015

Wang, M., Guan, Y., Zhang, J., Zhou, N., & Lu, S. (2020). Oil charging model and controlling factors revealed by an online nuclear magnetic resonance (NMR) system. *Marine and Petroleum Geology*, *118*, 104442. https://doi.org/10.1016/j.marpetgeo.2020.104442

Wang, M., Xue, H., Tian, S., Wilkins, R. W. T., & Wang, Z. (2015). Fractal characteristics of upper cretaceous lacustrine shale from the Songliao basin, NE China. *Marine and Petroleum Geology*, *67*, 144–153. https://doi.org/10.1016/j.marpetgeo.2015.05.011

Wang, S., Han, X., Dong, Y., & Shi, H. (2017). Mechanisms of reservoir pore/throat characteristics evolution during long-term waterflooding. *Advances in Geo-Energy Research*, *1*, 148–157. https://doi.org/10.26804/ager.2017.03.02

Wang, Y., Mckinzie, J., Furtado, F., & Aryana, S. (2020). Scaling Analysis of two-phase flow in fractal permeability fields. *Water Resources Research*, *56*, e2020WR028214. https://doi.org/10.1029/2020WR028214

Wei, W., Cai, J., Hu, X., & Qi, H. (2015). An electrical conductivity model for fractal porous media. *Geophysical Research Letters*, *42*, 4833–4840. https://doi.org/10.1002/2015GL064460

Wei, W., Zhang, C., Zhang, S., Wu, C., & Yang, K. (2016). Study on the cretaceous turbidite and reservoir features in the Qingshankou Formation in northern Songliao Basin, NE China. *Marine and Petroleum Geology*, *78*, 797–806. https://doi.org/10.1016/j.marpetgeo.2016.01.016

Wong, P., Howard, J., & Lin, J. S. (1986). Surface roughening and the fractal nature of rocks. *Physical Review Letters*, *57*, 637–640. https://doi.org/10.1103/PhysRevLett.57.637

Yang, Z., & Mohanty, B. P. (2015). Effective parameterizations of three nonwetting phase relative permeability models. *Water Resources Research*, *51*, 6520–6531. https://doi.org/10.1002/2014WR016190

Yu, B., Zou, C., Zou, Q., Cai, J., & Zheng, Q. (2014). *Transport physics of fractal porous media*. Science Press.

Zhang, L., Ba, J., & Carcione, J. M. (2021). Wave propagation in infinituple-porosity media. *Journal of Geophysical Research: Solid Earth*, *126*, e2020JB021266.

Zhang, L., Ba, J., Carcione, J. M., & Fu, L. Y. (2020). Differential poroelasticity model for wave dissipation in self-similar rocks. *International Journal of Rock Mechanics and Mining Sciences*, *128*, 104281.

Zhou, N., Lu, S., Wang, M., Liu, W., & Wang, Z. (2020). Applicability of fractal capillary pressure models to sandstones. *Journal of Petroleum Science and Engineering*, *185*, 106626. https://doi.org/10.1016/j.petrol.2019.106626

Zhu, X. (2008). *Sedimentary petrology*. Petroleum Industry Press.